Rational design of all resistive multifunctional sensors with stimulus discriminability

Jeng-Hun Lee, Eunyoung Kim, Heng Zhang, Haomin Chen, Harun Venkatesan, Kit-Ying Chan, Jie Yang, Xi Shen, Jinglei Yang, Seokwoo Jeon and Jang-Kyo Kim**

J. H. Lee, E. Kim, H. Zhang, H. Chen, Dr. H. Venkatesan, Dr. K. Y. Chan, Dr. J. Yang, Prof J. Yang, Prof J. K. Kim
Department of Mechanical and Aerospace Engineering, The Hong Kong University of Science and Technology, Clear Water Bay, Kowloon, Hong Kong
E-mail: mejkkim@ust.hk (J. K. Kim)

H. Chen, Prof. S. Jeon
Department of Materials Science and Engineering, Graphene Research Center of KI for the NanoCentury, Korea Advanced Institute of Science and Technology, Daejeon 305–338, Republic of Korea

X. Shen
Department of Aeronautical and Aviation Engineering The Hong Kong Polytechnic University Hung Hom, Kowloon, Hong Kong
E-mail: xi.shen@polyu.edu.hk (X. Shen)

Keywords: multifunctional sensor, pressure sensor, temperature sensor, stimulus discriminability, decoupling

A rational approach is proposed to design soft multifunctional sensors capable of detection and discrimination of different physical stimuli. Herein, a flexible multifunctional sensor concurrently detecting and distinguishing minute temperature and pressure stimuli in real time is developed using electrospun carbon nanofiber (CNF) films as the sole sensing material and electrical resistance as the only output signal. The stimuli sensitivity and discriminability are coordinated by tailoring the atomic- and device-level structures of CNF films to deliver outstanding pressure and temperature sensitivities of -0.96 $k\text{Pa}^{-1}$ and -2.44 $\%\text{°C}^{-1}$, respectively, enabling mutually exclusive sensing performance without signal cross-interference. The CNF multifunctional sensor is considered the first of its kind to accomplish the stimulus discriminability using only the electrical resistance as the output signal, which is most convenient to monitor and process for device applications. As such, it has distinct advantages over other reported sensors in its simple, cost-effective fabrication and readout system. It also possesses other invaluable traits, including good bending stability, fast response time and long-term durability. Importantly, the ability to simultaneously detect and decouple temperature and

pressure stimuli is demonstrated through novel applications as a skin-mountable device and a flexible game controller.

1. Introduction

Flexible multifunctional sensors capable of detecting important physical stimuli such as strain, pressure and temperature have gained major interests in recent years due to their promising applications in flexible electronics,[1–3] prosthesis development,[4–7] soft robotics[8–10] and healthcare devices.[11–14] To simultaneously monitor more than one type of physical stimuli, sensor networks consisting of multiple sensors should detect and decouple multiple sources of stimuli such as strain, pressure and temperature without interference among them.[15–17] Generally, the state-of-the-art flexible multifunctional sensors are designed to detect and decouple different combinations of various physical stimuli, for examples strain and temperature,[15] bending and pressure,[18] tactile and touchless interaction,[19] and pressure and temperature.[20] Among them, the multifunctional sensors capable of detecting and decoupling pressure and temperature stimuli have gained increasing interests in an effort to duplicate the indispensable pressure and temperature sensing capability of human skin, the largest sensory organ of a human body.[18,19] Yet, realizing the concurrent detection and decoupling of pressure and temperature stimuli using the same type of output signal from a given flexible sensor is a daunting challenge.[19–21]

Recently, a number of attempts have been made towards employing different materials or computer programs to develop flexible multifunctional sensors equipped with differentiating between dissimilar temperature and pressure stimuli. One strategy is to utilize thermoelectric[5,23,24] or ferroelectric[25] materials to fabricate multifunctional single sensors that can decouple temperature and pressure stimuli using their thermoelectric and piezoresistive[5,23,24] or pyroelectric and piezoelectric properties,[25] respectively. However, temperature sensors (TSs) made of these materials commonly suffer from a lower sensitivity than those made from thermoresistive materials.[15,26] Further, the use of these materials

inevitably requires intricate readout systems to analyze current-voltage outputs of the sensors,[5,15] hindering their adoption for widespread commercial applications. Another strategy is to use machine learning (ML) or deep learning (DL) to distinguish different physical stimuli from coupled output data of multifunctional sensors.[27,28] Nevertheless, implementing either ML or DL requires post-acquisition data processing which in turn makes the overall readout system complicated. An alternative strategy is to integrate individual sensors exhibiting distinctive responses towards specific stimuli into a single device.[20,29] For this purpose, resistive temperature sensors (TSs) and capacitive pressure sensors (PSs) are commonly stacked for multifunctional sensing, making use of their respective pressure and temperature insensitivity.[20,29,30] Despite their simple device structures, however, the various materials required to produce individual sensors make the overall fabrication process complex and uneconomical. Moreover, utilization of two different sensors with different functions entails analyzing two different outputs, necessitating an elaborate signal processing and readout system.[20,22] Therefore, it is highly desired to develop sensitive multifunctional sensors having stimulus discriminability and yet benefiting from simple, cost-effective fabrication and readout systems, for instance, a multifunctional sensor whose outputs are only given in electrical resistance signals.[31] However, such all resistive multifunctional sensors capable of stimulus discriminability have rarely been reported to date because conductive fillers, such as graphene,[32–34] carbon nanotubes[35–37] and metal nanoparticles,[38–40] which are commonly used in the resistive PSs are known to exhibit significant sensitivity to temperature arising from their thermoresistive characteristics.[26,41]

This paper is dedicated to developing flexible, all resistive multifunctional sensors which can simultaneously detect and discriminate temperature and pressure stimuli in real time, using carbon nanofiber (CNF) films as the sole sensing material. Importantly, CNFs were produced *via* a facile, low-cost, and scalable electrospinning technique[2,42] and the sensors were constructed using them with an extremely simple readout system having electrical resistance as

the sole output. By exploiting the sensing mechanisms of CNFs associated with their different structures at the atomic and device levels, two types of CNF films with distinctive architectures were integrated into a multifunctional sensor, generating two signals of the same kind, namely electrical resistance, to measure the temperature and pressure independently. The multifunctional sensors made from the CNF films exhibited outstanding pressure and temperature sensitivities of -0.96 $k\text{Pa}^{-1}$ and -2.44 $\%^{\circ}\text{C}^{-1}$, respectively, without signal interference. In addition, the sensors delivered stable performance even after repeated bending cycles, good response time, and excellent durability. Finally, we demonstrated their capability to simultaneously detect and decouple temperature and pressure stimuli by means of a skin-mountable device and a flexible game controller.

2.1. Fabrication of Multifunctional Sensors Using Electrospun CNF Films

Figure 1a shows the fabrication process of CNF films using an electrospinning method. Briefly, 10 wt% polyacrylonitrile (PAN) precursor solution was electrospun on a drum collector. The high voltage applied between the syringe needle and the collector enabled the PAN precursor to be ejected onto the rotating collector to form a nanofiber web with uniform thickness.[42] The electrospun polymer nanofiber film was peeled from the collector, stabilized at 230 ℃ in air and carbonized at different temperatures ranging from 550 to 1000 ℃ in an Ar atmosphere, designated as CNF550, CNF1000 and so on. These CNF films of ~ 100 μm in thickness consisted of nanofibers with an average diameter of ~ 250 nm independent of carbonization temperature (CT) (Figure S1). They were freestanding with excellent flexibility, as shown in Figure 1b.

Flexible multifunctional sensors were constructed by stacking several layers of these CNF films and encapsulated in a protective polymer film, as illustrated in Figure 1c. Interestingly, these sensors showed distinctive temperature and pressure sensitivities depending on CT and the number of CNF layers (N), making it possible to produce both TSs and PSs by tailoring these parameters. First, as the CT increased, the CNF films showed diminishing thermoresistive

characteristics. Thus, the electrical resistance of CNF films carbonized at 1000 ℃ exhibited negligible changes to temperature variation, demonstrating temperature insensitivity. Second, the CNF films showed diminishing piezoresistive sensitivities with decreasing *N*, meaning that the CNF film with N = 1 displayed a negligible electrical resistance change upon pressure application, i.e., pressure insensitivity. Therefore, a temperature-insensitive PS was assembled using multilayer CNF films produced at a high CT of 1000 °C, while a pressure-insensitive TS was fabricated using a mono-layer CNF film produced a low CT of 550 °C. Ultimately, a sensible approach was devised in this work, such that a flexible bimodal CNF sensor having both excellent sensitivity and discriminability towards temperature and pressure stimuli was prepared by simply stacking the TS on top of the PS, as shown in Figure S2.

2.2. Performance of the All Resistive CNF Multifunctional Sensor with Stimulus Discriminability

The CNF multifunctional sensor consisting of the TS made of a mono-layer CNF550 film and the PS made of tri-layer CNF1000 films delivered remarkable temperature and pressure sensitivities of -2.44 %℃$^{-1}$ and -0.96 *k*Pa^{-1} in the ranges of 25-50 ℃ and 0-0.4 *k*Pa, respectively (**Figures 2**a and b). The temperature range of 25-50 ℃ and the pressure range of 0-2.0 *k*Pa were selected as the working range of the sensor to match the temperature and pressure ranges in human body applications.[11,12] The working principles and performance of these two component sensors for stimulus discriminability are elaborated below. First, the TS comprising a CNF550 film imparted a much larger variation in relative electrical resistance change ($\Delta R/R_0$) for a given temperature rise than those made of CNF films prepared at higher CTs (Figures S3a). The temperature coefficient of resistance (TCR) is a measure of the sensitivity of a resistive TS and is given by:[33,43]

$$TCR = \frac{\Delta R_{TS}/R_{TS,0}}{\Delta T} \times 100\ \% \quad (1)$$

where ΔR_{TS} is the total resistance change upon temperature variation, ΔT, and $R_{TS,0}$ is the initial resistance of the TS. The TCRs of the TSs made of different CNF films are compared in Figure S3b. It increased continuously as the CT decreased, reaching a maximum of 2.44 %°C^{-1} for the CNF550 TS. The TCRs of the TSs in the temperature range from 25 to 50 °C were calculated directly using Equation (1) as their $\Delta R/R_0$ presented an almost linear variation with temperature in this range (Figure S3a). In fact, the temperature sensing range of the CNF550 TS could be reasonably extended to 85 °C, as displayed in Figure S4. Further lowering the CT below 550 °C yielded extremely large $R_{TS,0}$ of over 100 MΩ, making the sensor less attractive for practical applications because a very high voltage would be required to drive the sensor (Figure S5). Second, tri-layers of the CNF1000 films were utilized to fabricate the PS because they offered the highest pressure sensitivity given the ease of fabrication and the low production cost. Typically, the sensitivity of the resistive PS, namely the pressure coefficient of resistance (PCR), is measured by:[44]

$$PCR = \frac{\Delta R_{PS}/R_{PS,0}}{\Delta p} \times 100\ \% \qquad (2)$$

where ΔR_{PS} is the total resistance change upon pressure variation, Δp, and $R_{PS,0}$ is the initial resistance of the PS. It was observed that the sensitivities of the PSs drastically improved as N increased from one to three, but further increasing N beyond three resulted in only negligible changes in pressure sensitivity (Figure S6). The sensitivities of the PSs were calculated by linear fitting their $\Delta R/R_0$ vs pressure curves in two different pressure regimes, one from 0 to 0.5 kPa and the other from 0.5 to 2.0 kPa, as shown in Figure 2b, by reasonably approximating the non-linear $\Delta R/R_0$ response. It is also worth noting that the pressure sensitivity of the CNF1000 PS could be reasonably extended to 10 *k*Pa: despite the rather lower sensitivity at higher pressures beyond 2 *k*Pa, the sensor presented a linear relationship between the electrical resistance change and pressure (Figure S7). Further, the CNF1000 PS demonstrated a decent sensing resolution,

successfully responding to a small pressure of 0.2 *k*Pa with a large decrease in its electrical resistance (Figure 2b).

In addition to the excellent temperature and pressure sensitivities, the CNF multifunctional sensor was able to decouple the responses from different stimuli, as shown in Figure 2c. It is clearly seen that $\Delta R/R_0$ of the CNF550 TS remained almost constant when the pressure was varied between 0 and 20 kPa while $\Delta R/R_0$ for the CNF1000 PS remained unchanged against temperature variation ranging 25-50 ℃. Further, the CNF550 TS exhibited essentially identical $\Delta R/R_0$ curves upon temperature variation regardless of the weight placed onto the sensor (Figure S8a). Meanwhile, the CNF1000 PS showed almost identical $\Delta R/R_0$ responses to pressure variation when it was heated with an infrared lamp compared to the room-temperature counterpart (Figure S8b). On one hand, the insensitivity to pressure was achieved by fully encapsulating the CNF550 film using polydimethylsiloxane (PDMS). To ensure complete infiltration of PDMS and thus achieve the pressure insensitivity of the CNF550 TS, a constant amount of PDMS was applied for spin coating of the CNF550 film followed by vacuum treatment for 10 min. The contact and tunneling areas between neighboring CNFs were marginally improved when a pressure was applied because the individual CNFs were completely separated by the infiltrated PDMS (Figure S9), contributing to the pressure insensitivity. On the other hand, the unique insensitivity to temperature emerged from the interplay between metallic and semiconducting segments of the CNFs carbonized at 1000 ℃, as discussed in detail in Section 2.3. The multifunctional sensor also exhibited excellent durability as attested by the identical $\Delta R/R_0$ curves from the 1st to 500th cycles of temperature variation between 25 and 50 ℃ (Figure 2d) and extremely stable $\Delta R/R_0$ variations with an almost constant minimum level during the entire 3000 pressure loading/unloading cycles (Figure 2e). Therefore, even though the multifunctional sensor exhibited non-linear responses, especially to pressure variation (Figures 2a and 2b), the applied temperature and pressure could be accurately measured by monitoring the electrical resistance changes of the TS and PS,

respectively. These sensors produced from different electrospinning batches delivered consistent temperature and pressure sensing performance (Figure S10),[45] exhibiting almost identical $\Delta R/R_0$ curves in the entire sensing ranges and excellent sensitivities below 50 ℃ and 0.5 *k*Pa. Despite the repeatable sensing performance in the lab-scale setup, however, the electrospinning technique involving random deposition of nanofibers may result in non-uniform CNF samples in the large-scale production, and hence potentially inconsistent sensing capabilities. Therefore, the processing parameters, like electric field, solution feeding rate, relative humidity, and collecting distance, should be carefully controlled to guarantee the uniformity of samples as much as possible.[42] In addition, their temperature and pressure sensing performance was hardly influenced by CNF films containing fibers with different diameters which were produced from different PAN precursor solutions (Figure S11).

The thermal response and recovery times of the multifunctional sensor were measured by monitoring its electrical resistance change after a water droplet ~ 1℃ warmer than the room temperature was applied onto the sensor surface (Figure 2g). The sensor almost instantaneously responded with a resistance change in 0.73 s, highlighting its quick response to detect even a small temperature variation. This also meant that the sensor possessed a reasonable temperature sensing resolution of about 1 ℃. As the water temperature slowly approached the ambient temperature, the electrical resistance of the sensor fully returned to its initial value in 9.28 s, demonstrating a good recovery for a consistent sensing capability. The thermal recovery time was much longer than the response time because the entrapped heat in the PDMS matrix dissipated slowly *via* natural convection and due to the low thermal conductivity of PDMS.[25,44] The thermal recovery of the sensor could be made faster by applying a thinner PDMS encapsulation layer[23] or by adding high thermally conductive fillers like boron nitride nanosheets in the PDMS matrix.[47] These measures may also improve the sensitivity of the CNF550 TS because a thick PDMS layer potentially serves as thermal insulation, deteriorating its sensitivity. Moreover, the multifunctional sensor showed ultra-fast response and recovery

times of 0.18 and 0.05 s to an applied pressure of 0.4 *k*Pa, respectively (Figure 2h). Finally, the sensor also possessed excellent bending stability, as shown in Figure 2i. Its temperature and pressure sensing performance was barely affected even after 1000 bending/straightening cycles, a reflection of intrinsic flexibility of the freestanding electrospun CNF film.[46,48]

Overall, to the best of the authors' knowledge, the flexible CNF bimodal sensor presented here is the first of its kind capable of distinguishing minute temperature and pressure stimuli using the electrical resistance as the only type of output signal. The electrical resistance is known to be among the most convenient digital signals to monitor and process.[49] Moreover, the sensor is assembled using electrospun CNFs as the sole sensing component *via* an extremely simple fabrication process. Therefore, when compared to other state-of-the-art multifunctional sensors with stimulus discriminability reported in literature, the current flexible CNF multifunctional sensor has distinct advantages in its simple, cost-effective readout system and fabrication with balanced sensitivities between temperature and pressure, as summarized in Table S1.

2.3. Thermoresistive and Piezoresistive Mechanisms of the CNF Multifunctional Sensor with Stimulus Discriminability

The thermoresistive characteristics of electrospun PAN-based CNFs were proven to be highly correlated with their atomic structures.[26] The atomic structures of CNFs carbonized at different temperatures were dissected to explain the temperature-insensitive feature of the CNF1000 PS. The transmission electron microscopy (TEM) images of CNF550 and CNF1000 indicate that CNF550 was mostly amorphous in nature while partially aligned graphitic sp^2 domains appeared in CNF1000 (**Figure 3**a). The higher degree of graphitization in CNF1000 than in CNF 550 was confirmed by the X-ray powder diffraction (XRD) patterns. When the CT was increased from 550 to 1000 ℃, the broad prominent peak at around 25° upshifted slightly (Figure S12a), while the sp^2 carbon crystallite doubled its size from 0.57 to 1.10 *nm* (Figure 3b). The higher CT significantly reduced the D- to G-band intensity ratio, I_D/I_G, of Raman spectra from 1.43 to 0.83 (Figures 3c and S12b). These findings corroborate with a higher

carbon content and a reduced nitrogen content for CNF1000 than CNF550 according to the X-ray photoelectron spectroscopy (XPS) results (Figure S12c). Interestingly, among the three types of nitrogen functional groups, namely pyridinic-N (398.3 eV), pyrrolic-N (400.1 eV) and graphitic-N (403.4 eV), the pyridinic-N content dropped significantly, whereas the contents of the other two species increased with increasing CT (Figures 3d and e).[2,50]

The CNF550 TS exhibited a notable negative temperature coefficient (NTC) of resistance due to the small and randomly-oriented sp^2 crystallites, a large number of defects and a high pyridinic-N content.[26] Compared to CNF550, more segments of CNF1000 were metallic because of the improved alignment of sp^2 domains and larger crystallite sizes. The metallic nature typically yielded a positive temperature coefficient (PTC) where the electrical resistance increased with increasing temperature because of the enhanced atomic vibrational energy and thus augmented collision of free electrons.[26,51] Meanwhile, a smaller number of defects and a lower pyridinic-N content in CNF1000 translated into fewer entrapped and localized electrons, suppressing the NTC characteristic compared to CNF550. Therefore, the PTC feature of the metallic segment counterbalanced most of its NTC characteristic,[26] leading to an insensitive response of the CNF1000 PS to the temperature stimulus.

The piezoresistive mechanisms of the CNF1000 PSs containing different layers of CNF1000 films are illustrated in **Figure 4**. In the case of $N = 1$, the individual CNFs inside a mono-layer CNF film were closely packed, either already in physical contacts or only marginally separated (Figure 4a and S1). Therefore, the external pressure could barely increase the contact area between the individual CNFs in a CNF film, leading to a limited decrease in $\Delta R/R_0$ (Figure S6). When a few layers of CNF films were stacked together to form PSs, in contrast, their flexible nature and uneven surface inevitably created a large number of micro-scale voids with loosely connected individual CNFs, being unable to form intimate physical contacts between the CNF films, as shown in Figures 4b and S13a.[52,53] The structure of the CNF550 TS was in sharp contrast with the CNF1000 PS, where the mono-layer CNF film was totally encapsulated in the

PDMS matrix (Figure S9b). Once a small pressure was applied, these voids were squeezed to enhance the contact between the CNF films, and consequently, $\Delta R/R_0$ of the PS dropped (Figure S6). When the applied pressure exceeded 0.5 *k*Pa, however, the sensitivity of $\Delta R/R_0$ reduction with pressure became lower because of saturated physical contacts between the CNF films (Figure S6). Once the large pressure exceeding 0.5 *k*Pa was removed from the sensor, the squeezed voids reappeared as shown in Figure S13b. Although there were many voids available throughout the entire structure when N was increased to 5, those present between the bottom layers of CNF films were not squeezed as effectively as in N = 3 for a given applied pressure (Figure 4c). Accordingly, the sensitivity of the CNF1000 PS was only marginally improved by increasing N from 3 to 5 (Figure S6), similar to the trend observed in other multilayered resistive PSs.[52,54]

2.4. Applications of the CNF Multifunctional Sensor with Stimulus Discriminability

The CNF multifunctional sensor for bimodal temperature and pressure sensing was constructed by simply stacking each of component sensors, the CNF550 TS and CNF1000 PS. Its ability to simultaneously detect and distinguish the physical attributes was examined by monitoring $\Delta R/R_0$ of the two component sensors when subjected to different external stimuli (**Figures 5**a-c). First, when the multifunctional sensor was pressed with a finger, $\Delta R/R_0$ of both the CNF550 TS and CNF1000 PS decreased simultaneously (Figure 5a). Interestingly, when it was pressed with a plastic rod whose temperature was the same as the room temperature, only the CNF1000 PS responded with a drop in resistance while the CNF550 TS remained unaffected by the pressure (Figure 5b). In contrast, once the multifunctional sensor was blown with warm air, $\Delta R/R_0$ of the PS remained constant but that of the TS declined (Figure 5c). The above demonstrations signify that the CNF multifunctional sensor could monitor both pressure and temperature variations without any interference between the two signals, enabling mutually exclusive sensing performance by the two component sensors. It is also important to note that the CNF multifunctional sensor was highly flexible (Figure 5d) and as such, it could be easily

attached onto a human body to monitor the body temperature as well as small muscle movements (Figure 5e). When the sensor was attached to the forearm, $\Delta R/R_0$ of the TS component decreased until equilibrium was reached while that of the PS component showed no change (Region 1, Figure 5e), verifying successful detection of body temperature by the CNF multifunctional sensor. When the hand was clenched and spread out, the small forearm muscle movements were detected by the PS component where its $\Delta R/R_0$ continuously altered with the muscle movements (Region 2, Figure 5e). Notably, these movements did not create any crosstalk nor signal change in the TS component.

Because all outputs of the CNF multifunctional sensor are depicted in electrical resistance, it could be directly connected to an Arduino board and used as a flexible game controller. With the aid of simple coding, the CNF multifunctional sensor was designed to be activated only when the $\Delta R/R_0$ values of both the TS and PS components fell within a certain range, as highlighted in **Figure 6**a. In other words, the flexible CNF multifunctional sensor was tuned such that it would be 'on' only when pressed with a finger while remained 'off' under other external stimuli (Figure 6a and Video S1, Supporting Information). In this demonstration, the game called "T-rex Runner" could only be executed when the sensor was pressed with a finger. Moreover, the CNF multifunctional sensors could easily be made into an array (Figure S14a) while preserving their rollable and flexible nature (Figures S14b and c). The array of three CNF multifunctional sensors was successfully used to play a more complex game, "Red Runner", as shown in Figure 6b and Video S2, Supporting Information. Summarizing, the CNF multifunctional sensor was capable of distinguishing the pressure arising from a human finger and other objects by assessing the collective resistance responses from the TS and PS components thanks to their distinct and highly selective responses towards temperature and pressure, respectively.

3. Conclusion

In summary, this paper reports the rational structural design of electrospun CNFs at both the atomic and device levels towards all resistive multifunctional sensors capable of simultaneously detecting and distinguishing temperature and pressure without signal crosstalk. Notably, high stimulus discriminability was achieved by using only one type of output signal, namely the electrical resistance, which is among the most convenient digital signals to track and process for device applications. Moreover, the multifunctional sensor was assembled using solely the CNF films as the sensing material produced based on a simple and scalable electrospinning process. As a result, the CNF multifunctional sensor had distinct advantages in its simple, cost-effective readout system and fabrication. Thanks to the unique sensing mechanisms associated with the atomic- and device-level structures of the CNF sensors, two independent sensing units comprised the multifunctional sensor for detecting temperature and pressure simultaneously, enabling mutually exclusive sensing performance between them. A single layer CNF film carbonized at 550 ℃ served as TS to monitor temperature without being interfered by the pressure, whereas a tri-layer CNF film carbonized at 1000 ℃ functioned as PS to detect pressure while unaffected by temperature. Successful tuning of the CNF structure and the number of CNF films facilitated both the component sensors to operate in a desired manner. The multifunctional sensor exhibited outstanding pressure and temperature sensitivities of -0.96 $k\text{Pa}^{-1}$ and -2.44 $\%\text{℃}^{-1}$, respectively, without cross-interference between the two stimuli. In addition, it showed excellent bending stability, fast response time and superior durability. Its novel, potential applications were demonstrated as a skin-mountable device to monitor body temperature as well as small muscle movements, and a flexible game controller to play T-rex Runner and Red Runner. Overall, our all resistive multifunctional sensor with stimulus discriminability offers a new sensing platform possessing a simplified signal processing capability for more advanced applications of flexible electronics in the future.

4. Experimental Section

Preparation of CNF films: The CNF film was produced *via* electrospinning according to our previous study.[26,55] The precursor polymer was prepared by dissolving 10 wt% PAN (average M_w = 150 k supplied by Aldrich) in 10 mL N,N-dimethylformamide (DMF) at 80 ℃ for 3 h under magnetic stirring. The solution was electrospun using a spinning machine (KATO Tech. Co., Japan) at 14 kV, and the distance between the needle and the collector was kept constant at 150 mm. The flow rate was maintained at 1.0 mL h^{-1} using a 19-gauge stainless steel needle. The PAN nanofiber film was prepared on a drum collector at a rotational speed of 0.5 m min^{-1}. The relative humidity was kept below 40 % throughout the electrospinning process. The PAN nanofiber film was stabilized at 230 ℃ for 3 h in an air-circulated oven, followed by carbonization at different temperatures ranging from 550 to 1000 ℃ for 1 h at a ramp rate of 2 ℃ min^{-1} in an Ar atmosphere to obtain the CNF films.

Fabrication of the CNF multifunctional sensor: First, the CNF550 TS was prepared by encapsulating a CNF550 film in a PDMS matrix. PDMS (Sylgard184, Dow Corning, base: curing agent = 10:1 by weight) solution was stirred for 20 min at room temperature, followed by degassing in a vacuum oven for 30 min. A thin PDMS film was prepared by spin coating at 1200 rpm for 15 s and precured in an oven at 80 ℃ for 5 min. The freestanding CNF550 film was cut into a square of 15 mm × 15 mm and was transferred onto the precured PDMS film. After curing at 80 ℃ for 10 min, silver paste was applied at both ends of the CNF550 film to connect to copper wires. Another PDMS layer was spin coated on top using a constant amount of PDMS resin, and the whole assembly was placed in vacuum for 10 min to ensure the complete infiltration of PDMS into the CNF550 film. The whole assembly was then cured at 80 ℃ for 10 min in an oven. Second, the CNF1000 PS was produced using multiple layers of the CNF1000 films. In detail, the CNF1000 film was cut into a square of 15 mm × 15 mm and stacked between the electrodes on polyethylene terephthalate (PET) substrates using 3M double-sided tapes of thickness ~ 300 μm. Third, the CNF550 TS was stacked on the CNF1000 PS to assemble the CNF multifunctional sensor.

Fabrication of the flexible game controller: A single or an array of CNF multifunctional sensor(s) was connected to a microcontroller (MCU, Arduino Leonardo). The changes in electrical resistance resulting from various physical stimuli were converted to digital data by the Arduino Leonardo signal processing circuit.

Characterization and Performance of the CNF multifunctional sensor: Scanning electron microscope (SEM, JEOL JSM-6390F and Hitachi TM3030) and transmission electron microscope (TEM, JEOL 2010) were used to examine the morphologies of the CNF films. Micro-Raman spectrometer (Renishaw Micro-Raman /Photoluminescence System) with a 514.5 nm Ar ion laser source at 10 mW was used to obtain Raman spectra of CNFs carbonized at different temperatures. The crystal structures of CNFs were studied using X-ray powder diffraction (XRD, PW1830, Philips) with CuK α radiation from 10 to 70 ° and their chemical compositions were characterized by X-ray photoelectron spectroscopy (XPS, PHI5600, Physical Electronics). The temperature sensing performance of the CNF multifunctional sensors was evaluated by placing them on a hot-plate and monitoring the electrical resistance changes using a digital multimeter (34970A Data Acquisition/Data Logger Switch Unit, Agilent). The pressure sensing performance of the multifunctional sensors was examined on a universal testing machine (MTS 12) where the digital multimeter was used to continuously record the corresponding changes in electrical resistance upon pressure application.

Supporting Information

Supporting Information is available from the Wiley Online Library or from the author.

Acknowledgements

This project was financially supported by the Research Grants Council (GRF projects: 16229216, 16209917, 16205517 and 16200720) and the Innovation and Technology Commission (ITS/012/19) of Hong Kong SAR. JHL is the recipient of the Hong Kong PhD Fellowship. Technical assistance from the Advanced Engineering Materials facilities (AEMF) and the Materials Characterization and Preparation Facilities (MCPF) is appreciated.

Received: ((will be filled in by the editorial staff))
Revised: ((will be filled in by the editorial staff))
Published online: ((will be filled in by the editorial staff))

References

[1] J. Shin, B. Jeong, J. Kim, V. B. Nam, Y. Yoon, J. Jung, S. Hong, H. Lee, H. Eom, J. Yeo, J. Choi, D. Lee, S. H. Ko, *Adv. Mater.* **2020**, *32*, 1905527.

[2] J.-H. Lee, J. Kim, D. Liu, F. Guo, X. Shen, Q. Zheng, S. Jeon, J.-K. Kim, *Adv. Funct. Mater.* **2019**, *29*, 1901623.

[3] H. Zhang, D. Liu, J.-H. Lee, H. Chen, E. Kim, X. Shen, Q. B. Zheng, J. Yang, J.-K. Kim, *Nano-Micro Lett.* **2021**, *13*, 122.

[4] M. Khatib, O. Zohar, W. Saliba, H. Haick, *Adv. Mater.* **2020**, *32*, 2000246.

[5] F. Zhang, Y. Zang, D. Huang, C. Di, D. Zhu, *Nat. Commun.* **2015**, *6*, 8356.

[6] R. Yin, D. Wang, S. Zhao, Z. Lou, G. Shen, *Adv. Funct. Mater.* **2021**, *31*, 2008936.

[7] S. Peng, S. Wu, Y. Yu, P. Blanloeuil, C. H. Wang, *J. Mater. Chem. A* **2020**, *8*, 20531.

[8] O. A. Araromi, M. A. Graule, K. L. Dorsey, S. Castellanos, J. R. Foster, W. Hsu, A. E. Passy, J. J. Vlassak, J. C. Weaver, C. J. Walsh, R. J. Wood, *Nature* **2020**, *587*, 219.

[9] X. Fu, L. Wang, L. Zhao, Z. Yuan, Y. Zhang, D. Wang, D. Wang, J. Li, D. Li, V. Shulga, G. Shen, W. Han, *Adv. Funct. Mater.* **2021**, *31*, 2010533.

[10] V. Sanchez, C. J. Walsh, R. J. Wood, *Adv. Funct. Mater.* **2021**, *31*, 2008278.

[11] J. C. Yang, J. Mun, S. Y. Kwon, S. Park, Z. Bao, S. Park, *Adv. Mater.* **2019**, *31*, 1904765.

[12] Q. B. Zheng, J.-H. Lee, X. Shen, X. Chen, J.-K. Kim, *Mater. Today* **2020**, *36*, 158.

[13] N. Luo, W. Dai, C. Li, Z. Zhou, L. Lu, C. C. Y. Poon, S.-C. Chen, Y. Zhang, N. Zhao, *Adv. Funct. Mater.* **2016**, *26*, 1178.

[14] Y. Yu, S. Peng, P. Blanloeuil, S. Wu, C. H. Wang, *ACS Appl. Mater. Interfaces* **2020**, *12*, 36578.

[15] F. Li, Y. Liu, X. Shi, H. Li, C. Wang, Q. Zhang, R. Ma, J. Liang, *Nano Lett.* **2020**, *20*, 6176.

[16] Z. Gao, Z. Lou, W. Han, G. Shen, *ACS Appl. Mater. Interfaces* **2020**, *12*, 24339.

[17] Y. Guo, X. Wei, S. Gao, W. Yue, Y. Li, G. Shen, *Adv. Funct. Mater.* **2021**, 2104288.

[18] R. Feng, Y. Mu, X. Zeng, W. Jia, Y. Liu, X. Jiang, Q. Gong, Y. Hu, *Sensors* **2021**, *21*, 1.

[19] J. Ge, X. Wang, M. Drack, O. Volkov, M. Liang, G. S. Cañón Bermúdez, R. Illing, C. Wang, S. Zhou, J. Fassbender, M. Kaltenbrunner, D. Makarov, *Nat. Commun.* **2019**, *10*, 4405.

[20] G. Y. Bae, J. T. Han, G. Lee, S. Lee, S. W. Kim, S. Park, J. Kwon, S. Jung, K. Cho, *Adv. Mater.* **2018**, *30*, 1803388.

[21] J. Rao, Z. Chen, D. Zhao, R. Ma, W. Yi, C. Zhang, D. Liu, X. Chen, Y. Yang, X. Wang, J. Wang, Y. Yin, X. Wang, G. Yang, F. Yi, *Nano Energy* **2020**, *75*, 105073.

[22] K. Xu, Y. Lu, K. Takei, *Adv. Funct. Mater.* **2020**, *2007436*, 1.

[23] P. Zhu, Y. Wang, Y. Wang, H. Mao, Q. Zhang, Y. Deng, *Adv. Energy Mater.* **2020**, *10*, 2001945.

[24] Y. Wang, H. Wu, L. Xu, H. Zhang, Y. Yang, Z. L. Wang, *Sci. Adv.* **2020**, *6*, eabb9083.

[25] K. Song, R. Zhao, Z. L. Wang, Y. Yang, *Adv. Mater.* **2019**, *31*, 1902831.

[26] J.-H. Lee, H. Chen, E. Kim, H. Zhang, K. Wu, H. Zhang, X. Shen, Q. Zheng, J. Yang, S. Jeon, J.-K. Kim, *Mater. Horizons* **2021**, *8*, 1488.

[27] J. H. Lee, J. S. Heo, Y. Kim, J. Eom, H. J. Jung, J. Kim, I. Kim, H. Park, H. S. Mo, Y. Kim, S. K. Park, *Adv. Mater.* **2020**, *32*, 2000969.

[28] K. K. Kim, I. Ha, M. Kim, J. Choi, P. Won, S. Jo, S. H. Ko, *Nat. Commun.* **2020**, *11*, 2149.

[29] Z. Gao, Z. Lou, W. Han, G. Shen, *ACS Appl. Mater. Interfaces* **2020**, *12*, 24339.

[30] J. C. Yang, J. O. Kim, J. Oh, S. Y. Kwon, J. Y. Sim, D. W. Kim, H. B. Choi, S. Park, *ACS Appl. Mater. Interfaces* **2019**, *11*, 19472.

[31] C. Wang, K. Xia, H. Wang, X. Liang, Z. Yin, Y. Zhang, *Adv. Mater.* **2019**, *31*, 1801072.

[32] G. Zu, K. Kanamori, K. Nakanishi, J. Huang, *Chem. Mater.* **2019**, *31*, 6276.

[33] A. Chhetry, S. Sharma, S. C. Barman, H. Yoon, S. Ko, C. Park, S. Yoon, H. Kim, J. Y. Park, *Adv. Funct. Mater.* **2021**, *31*, 2007661.

[34] Q. Wang, S. Ling, X. Liang, H. Wang, H. Lu, Y. Zhang, *Adv. Funct. Mater.* **2019**, *29*, 1808695.

[35] J. H. Cai, J. Li, X. D. Chen, M. Wang, *Chem. Eng. J.* **2020**, *393*, 124805.

[36] J. Zhou, X. Xu, Y. Xin, G. Lubineau, *Adv. Funct. Mater.* **2018**, *28*, 1705591.

[37] A. Di Bartolomeo, M. Sarno, F. Giubileo, C. Altavilla, L. Iemmo, S. Piano, F. Bobba, M. Longobardi, A. Scarfato, D. Sannino, A. M. Cucolo, P. Ciambelli, *J. Appl. Phys.* **2009**, *105*, 064518.

[38] H. Chen, Y. Jing, J. H. Lee, D. Liu, J. Kim, S. Chen, K. Huang, X. Shen, Q. B. Zheng, J. Yang, S. Jeon, J.-K. Kim, *Mater. Horizons* **2020**, *7*, 2378.

[39] H. Schlicke, S. Kunze, M. Rebber, N. Schulz, S. Riekeberg, H. K. Trieu, T. Vossmeyer, *Adv. Funct. Mater.* **2020**, *30*, 2003381.

[40] J. Bang, W. S. Lee, B. Park, H. Joh, H. K. Woo, S. Jeon, J. Ahn, C. Jeong, T. Kim, S. J. Oh, *Adv. Funct. Mater.* **2019**, *29*, 1903047.

[41] A. Haque, M. A. Al Mamun, M. F. N. Taufique, P. Karnati, K. Ghosh, *IEEE Trans. Semicond. Manuf.* **2018**, *31*, 535.

[42] B. Zhang, F. Kang, J. M. Tarascon, J. K. Kim, *Prog. Mater. Sci.* **2016**, *76*, 319.

[43] Q.-J. Sun, X.-H. Zhao, Y. Zhou, C.-C. Yeung, W. Wu, S. Venkatesh, Z.-X. Xu, J. J. Wylie, W.-J. Li, V. A. L. Roy, *Adv. Funct. Mater.* **2019**, *29*, 1808829.

[44] Y. Huang, X. Fan, S. Chen, N. Zhao, *Adv. Funct. Mater.* **2019**, *29*, 1808509.

[45] S. Pyo, J. Lee, W. Kim, E. Jo, J. Kim, *Adv. Funct. Mater.* **2019**, *29*, 1902484.

[46] C. Wang, K. Xia, M. Zhang, M. Jian, Y. Zhang, *ACS Appl. Mater. Interfaces* **2017**, *9*, 39484.

[47] F. Wang, X. Zeng, Y. Yao, R. Sun, J. Xu, C. P. Wong, *Sci. Rep.* **2016**, *6*, 1.

[48] S. Lee, A. Reuveny, J. Reeder, S. Lee, H. Jin, Q. Liu, T. Yokota, T. Sekitani, T. Isoyama, Y. Abe, Z. Suo, T. Someya, *Nat. Nanotechnol.* **2016**, *11*, 472.

[49] M. Amjadi, K. U. Kyung, I. Park, M. Sitti, *Adv. Funct. Mater.* **2016**, *26*, 1678.

[50] C. Zhang, L. Fu, N. Liu, M. Liu, Y. Wang, Z. Liu, *Adv. Mater.* **2011**, *23*, 1020.

[51] Z. Cui, F. R. Poblete, Y. Zhu, *ACS Appl. Mater. Interfaces* **2019**, *11*, 17836.

[52] L. Q. Tao, K. N. Zhang, H. Tian, Y. Liu, D. Y. Wang, Y. Q. Chen, Y. Yang, T. L. Ren, *ACS Nano* **2017**, *11*, 8790.

[53] L. Zhang, H. Li, X. Lai, T. Gao, J. Yang, X. Zeng, *ACS Appl. Mater. Interfaces* **2018**, *10*, 41784.

[54] L. Zhang, H. Li, X. Lai, T. Gao, X. Liao, W. Chen, X. Zeng, *Cellulose* **2019**, *26*, 5001.

[55] B. Zhang, Y. Yu, Z.-L. Xu, S. Abouali, M. Akbari, Y.-B. He, F. Kang, J.-K. Kim, *Adv. Energy Mater.* **2014**, *4*, 1301448.

[56] B. Muchharla, T. N. Narayanan, K. Balakrishnan, P. M. Ajayan, S. Talapatra, *2D Mater.* **2014**, *1*, 011008.

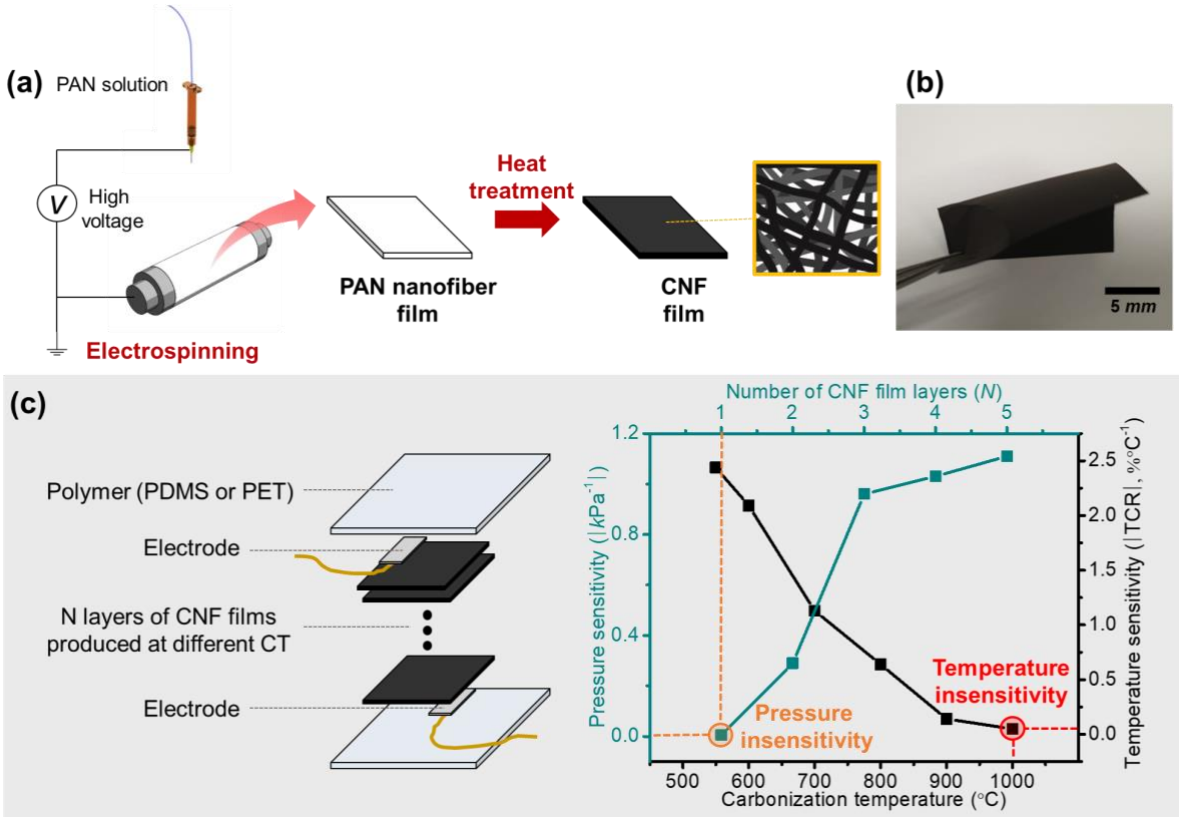

Figure 1. Fabrication of the multifunctional CNF sensors. (a) Schematic illustration showing the fabrication of CNF films by electrospinning and heat treatment. (b) Digital image of a freestanding CNF film demonstrating excellent flexibility. (c) Schematic showing the device structure of the CNF temperature and pressure sensors (TS, PS), and the correlation of carbonization temperature (CT) and *N* with temperature and pressure sensitivities, respectively. The temperature and pressure sensitivities were measured in the ranges of 25-50 ℃ and 0-0.4 *k*Pa, respectively, where the multifunctional sensor exhibited high linear responses to temperature and pressure variations, respectively.

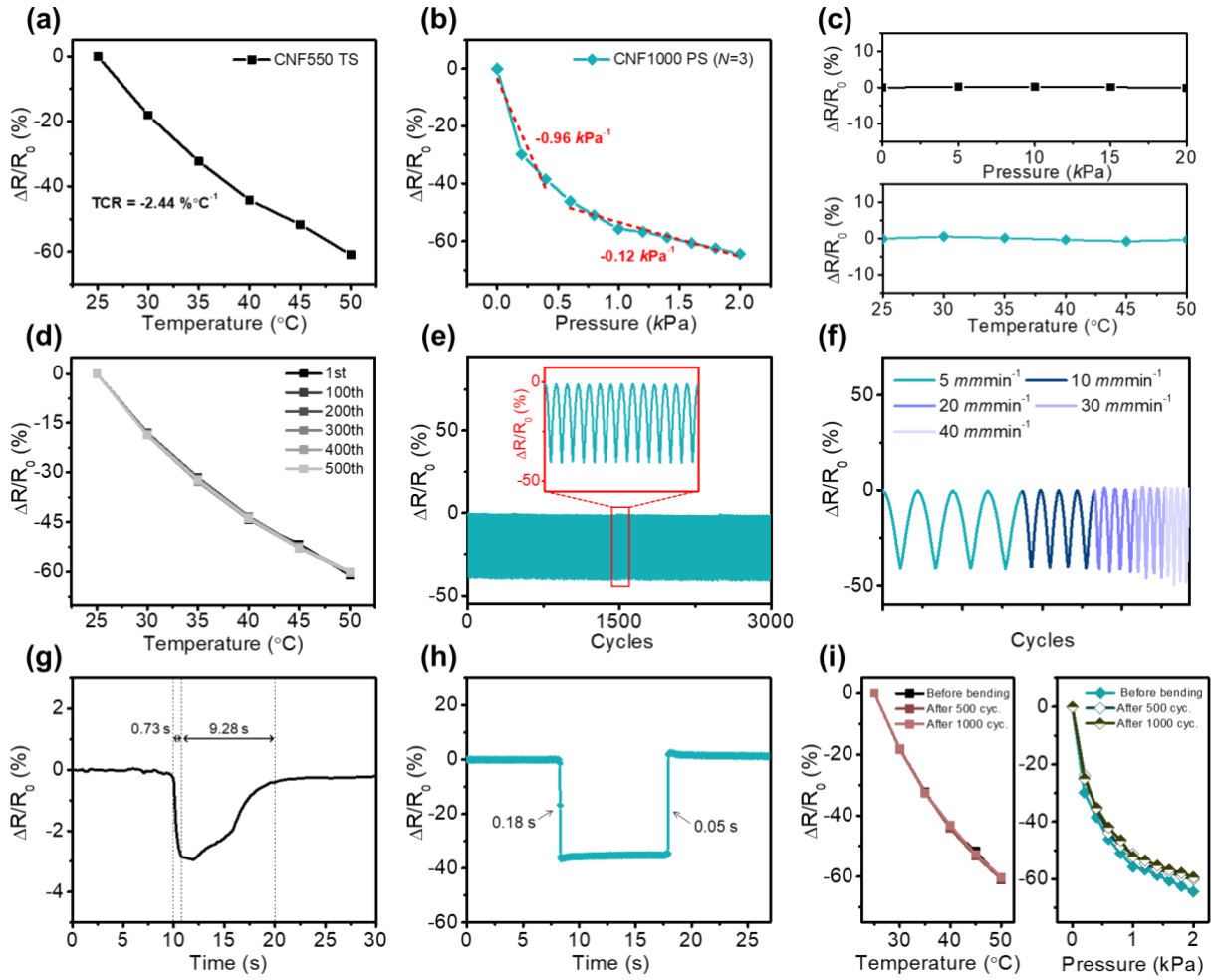

Figure 2. Performance of the CNF multifunctional sensor. (a) Temperature- and (b) pressure-dependent relative resistance changes ($\Delta R/R_0$) of the CNF550 TS and the CNF1000 PS in the CNF multifunctional sensor, respectively. (c) $\Delta R/R_0$ of the CNF550 TS and the CNF1000 PS in the CNF multifunctional sensor against pressure and temperature variations, respectively. (d-e) $\Delta R/R_0$ of the sensor against (d) temperature ranging from 25 to 50 ℃ for 500 cycles and (e) pressure variation to 0.4 *k*Pa for 3000 loading/unloading cycles, showing excellent durability. (f) $\Delta R/R_0$ of the sensor under 0.4 *k*Pa measured at different loading frequencies. (g) Thermal response and recovery times of the sensor measured by applying a water droplet ~ 1℃ warmer than the ambient on the sensor surface. (h) Mechanical response and recovery times of the sensor upon loading/unloading 0.4 *k*Pa pressure. (i) $\Delta R/R_0$ of the sensor against temperature and pressure variations after 500 and 1000 bending cycles.

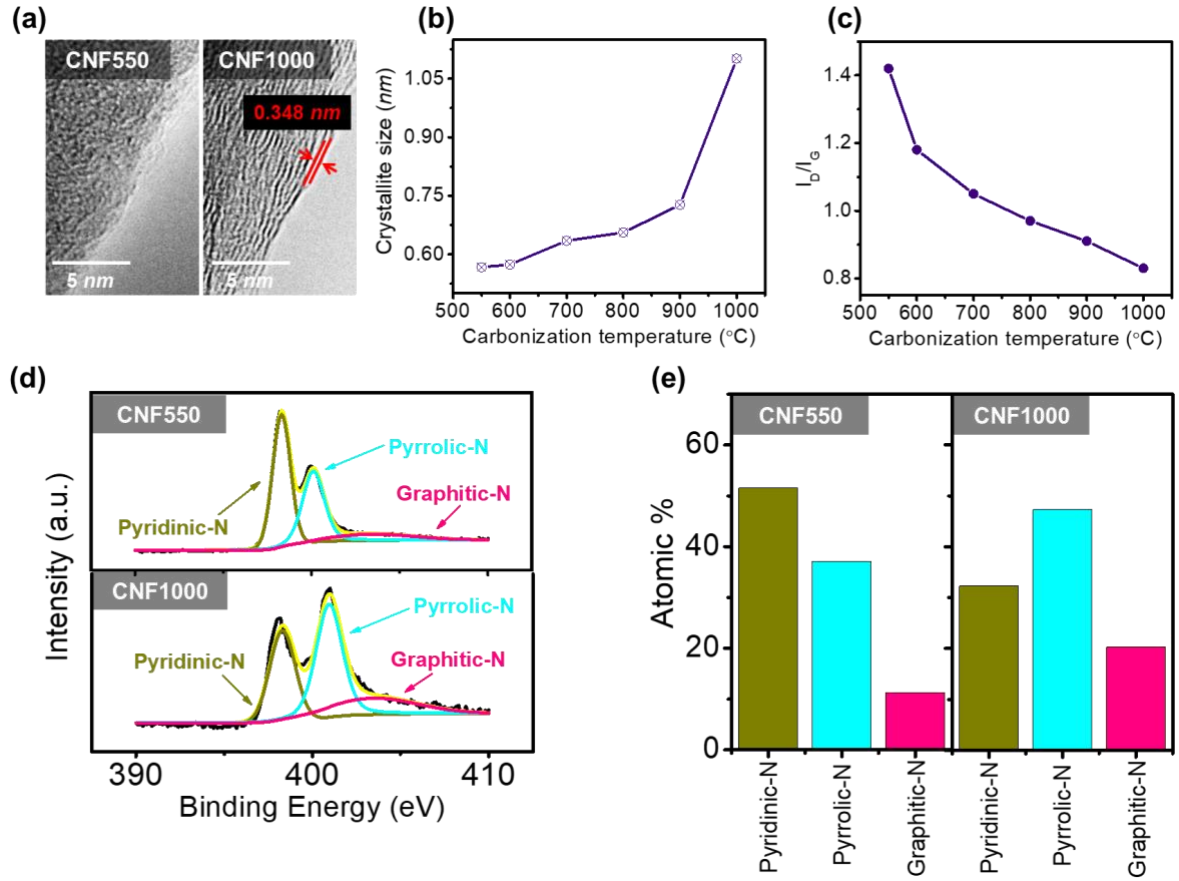

Figure 3. Atomic structures of CNFs carbonized at different temperatures. (a) TEM images of CNF550 and CNF1000, showing different sp^2 carbon structures. (b) Crystallite sizes of CNFs carbonized at different temperatures derived from XRD. (c) Raman I_D/I_G of CNFs carbonized at different temperatures. (d) Deconvoluted N1s spectra of CNF550 and CNF1000. (e) Atomic concentrations of pyridinic-N, pyrrolic-N and graphitic-N in CNF550 and CNF1000.

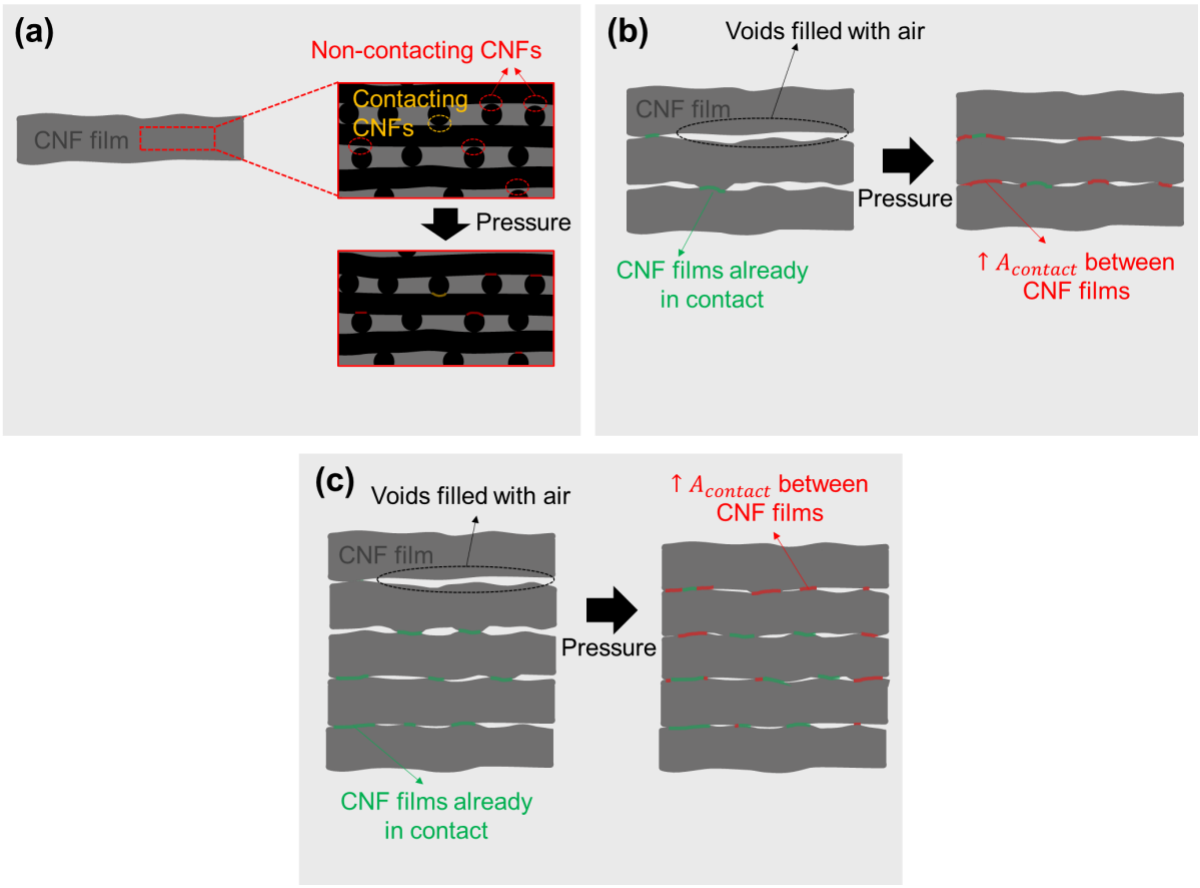

Figure 4. (a-c) Schematic illustrations showing the piezoresistive mechanisms of the CNF1000 PSs consisting of N = (a) one, (b) three and (c) five, respectively.

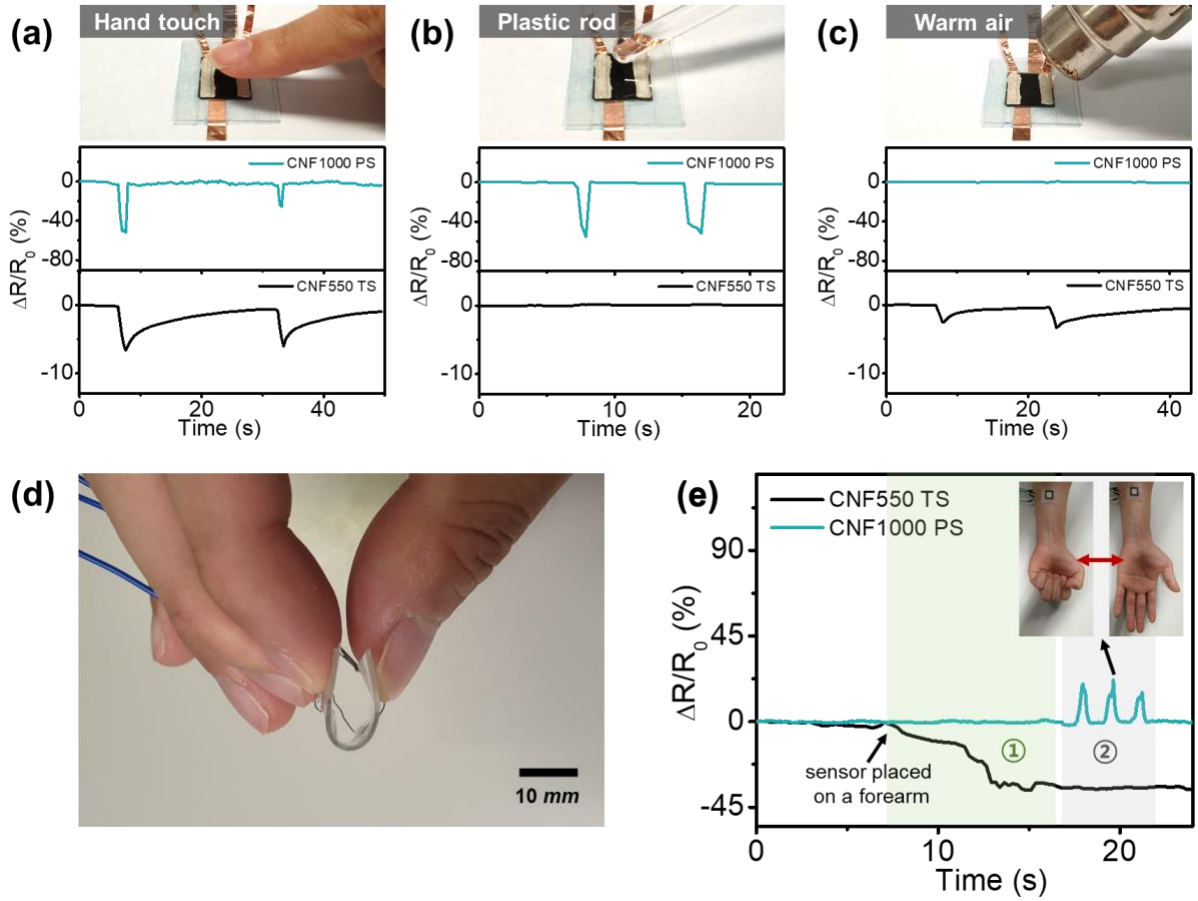

Figure 5. Mutually exclusive sensing performance of the component sensors in a CNF multifunctional sensor with stimulus discriminability. (a-c) variation of $\Delta R/R_0$ against time when stimulated with (a) a finger, (b) a plastic rod and (c) warm air. (d) Digital image of the bent sensor demonstrating excellent flexibility. (e) variation of $\Delta R/R_0$ against time when attached onto a human forearm to monitor body temperature and small forearm muscle movements.

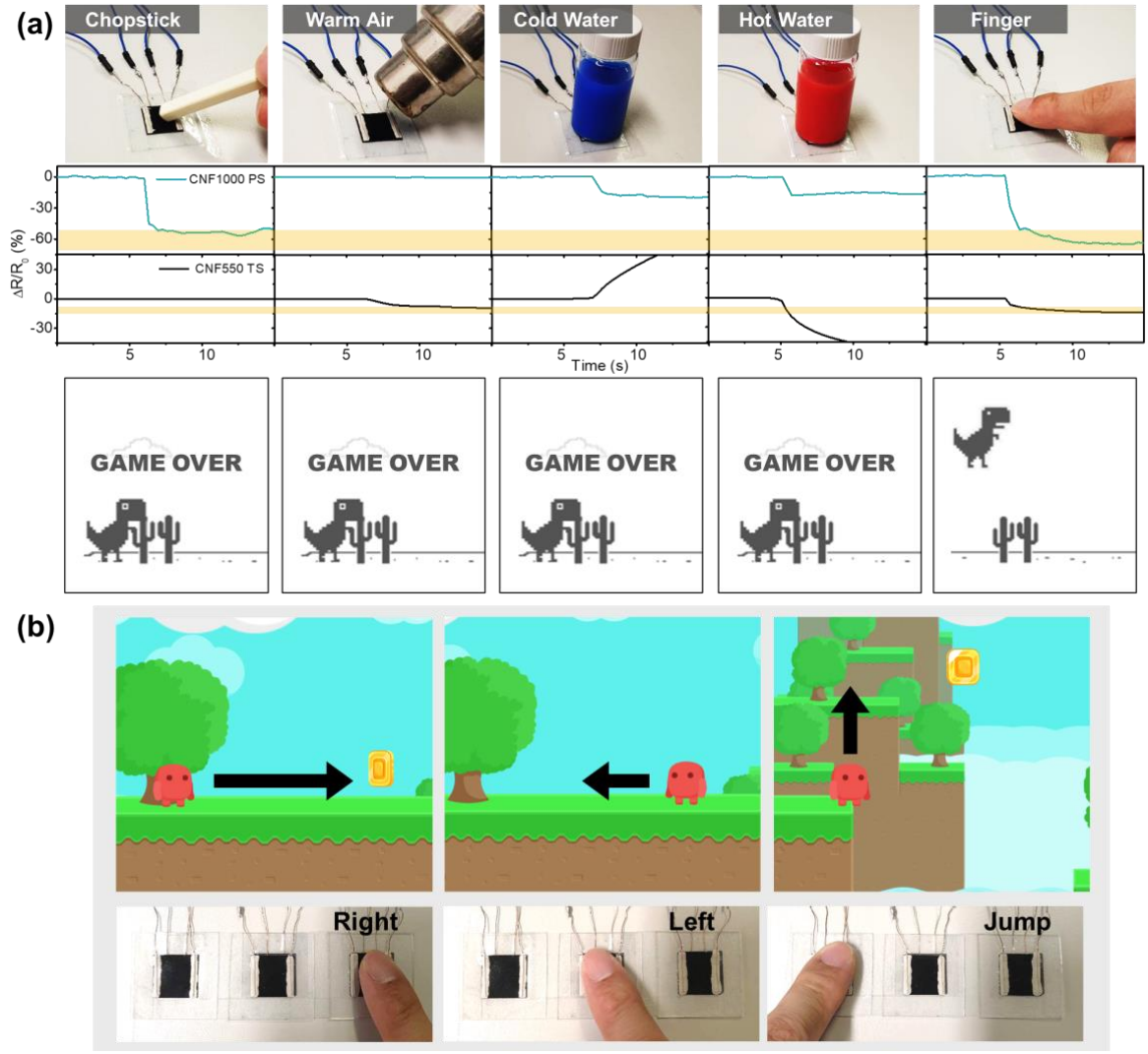

Figure 6. Applications of the CNF multifunctional sensor with stimulus discriminability, showing its potential as a flexible game controller. (a) Play demo of T-rex Runner using a single CNF multifunctional sensor, showing 'on' only when pressed with a human finger. (b) Play demo of Red Runner using the 1 × 3 array of three CNF multifunctional sensors. T-rex Runner reproduced with permission. Copyright Sebastien Gabriel. Red Runner reproduced under the Term of MIT License. Copyright 2017, Bayat Games.

A flexible multifunctional sensor capable of simultaneously detecting and discriminating temperature and pressure stimuli in real time is developed, exclusively using electrospun carbon nanofiber films as the sensing material. For the first time in the literature, it demonstrates a stimulus decoupling capability by means of monitoring electrical resistance as the sole and yet, most convenient digital signal.

Jeng-Hun Lee, Eunyoung Kim, Heng Zhang, Haomin Chen, Harun Venkatesan, Kit-Ying Chan, Jie Yang, Xi Shen, Jinglei Yang, Seokwoo Jeon and Jang-Kyo Kim**

Rational design of all resistive multifunctional sensors with stimulus discriminability

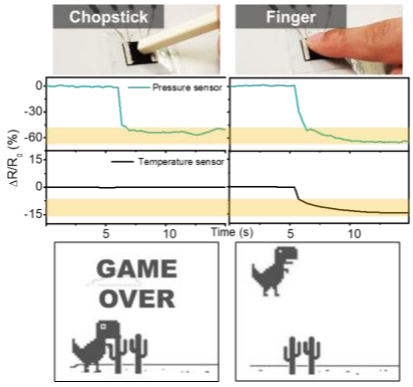

Supporting Information

Rational design of all resistive multifunctional sensors with stimulus discriminability

Jeng-Hun Lee, Eunyoung Kim, Heng Zhang, Haomin Chen, Harun Venkatesan, Kit-Ying Chan, Jie Yang, Xi Shen, Jinglei Yang, Seokwoo Jeon and Jang-Kyo Kim**

J. H. Lee, E. Kim, H. Zhang, H. Chen, Dr. H. Venkatesan, Dr. K. Y. Chan, Dr. J. Yang, Prof X. Shen, Prof J. Yang, Prof J. K. Kim
Department of Mechanical and Aerospace Engineering, The Hong Kong University of Science and Technology, Clear Water Bay, Kowloon, Hong Kong
E-mail: maeshen@ust.hk (X. Shen) mejkkim@ust.hk (J. K. Kim)

H. Chen, Prof. S. Jeon
Department of Materials Science and Engineering, Graphene Research Center of KI for the NanoCentury, Korea Advanced Institute of Science and Technology, Daejeon 305–338, Republic of Korea

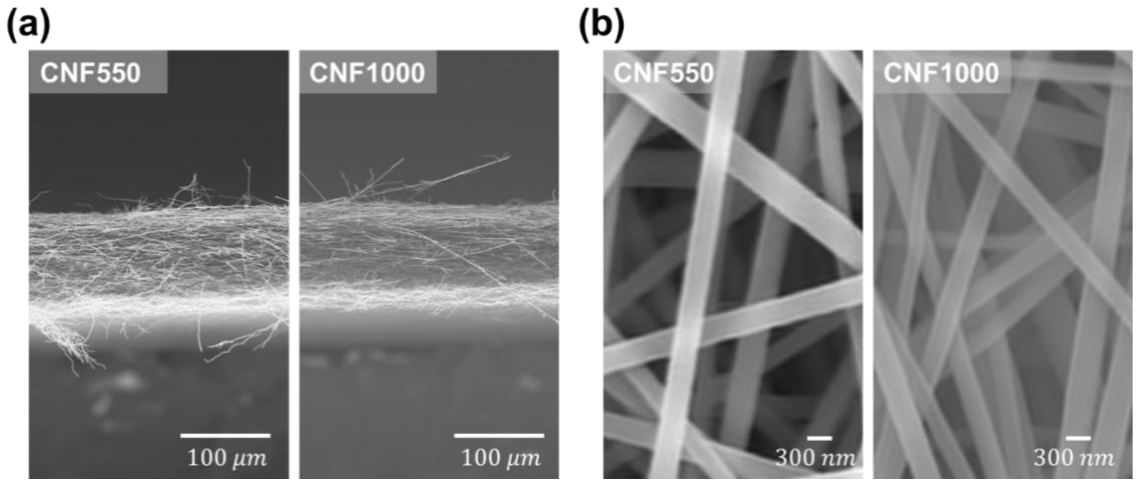

Figure S1. Scanning electron microscopic (SEM) images showing (a) the thicknesses and (b) the fiber diameters of the CNF550 and CNF1000 films, respectively.

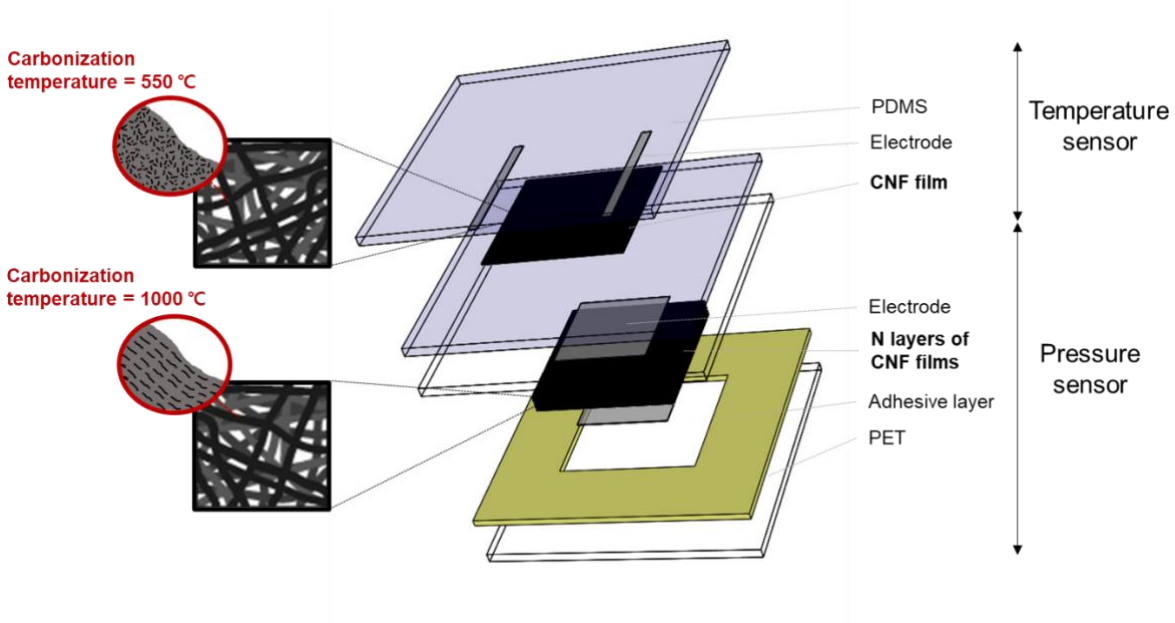

Figure S2. Schematic illustration of the flexible CNF multifunctional sensor with temperature and pressure stimuli discriminability.

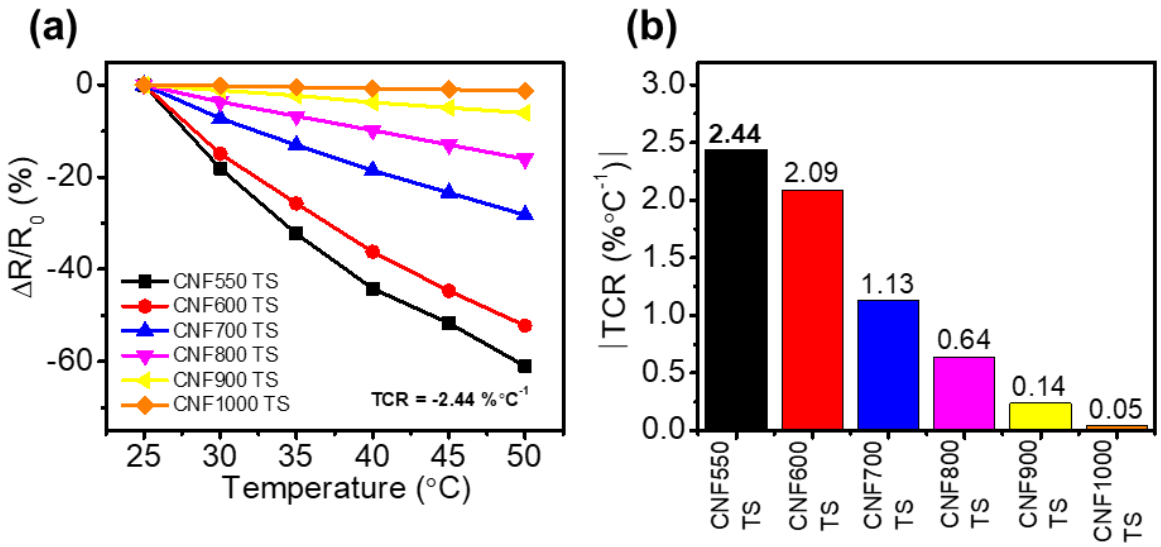

Figure S3. (a) Temperature-dependent $\Delta R/R_0$ and (b) the corresponding TCRs of the TSs made from CNF films carbonized at different temperatures.

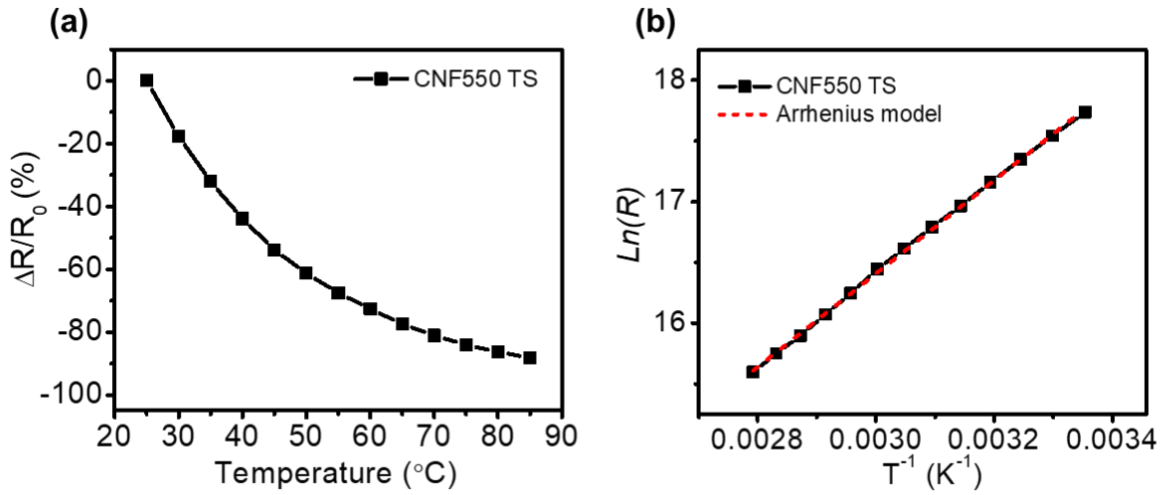

Figure S4. (a) Temperature-dependent $\Delta R/R_0$ in the temperature range from 25 to 85 °C and (b) plot of *ln* (R) vs T^{-1} for the CNF550 TS.

The CNF550 TS could satisfactorily function for temperature sensing at temperatures beyond 50 °C. Although the $\Delta R/R_0$ value presents a non-linear response at temperatures above 50 °C (Figure S4a), the thermoresistive response of the CNF550 TS is in good accordance with the Arrhenius model over the whole range of temperature from 25 to 85 °C (Figure S4b):[26,56]

$$ln(R) = ln(R_i) + \frac{E_a}{2kT} = ln(R_i) + \frac{B}{T} \quad \text{(S1)}$$

where R_i is the resistance of the TS at an infinite temperature, E_a is the activation energy, k is the Boltzmann constant, T is the temperature in Kelvins and B is the thermal index. Based on the above findings, it can be concluded that the thermally-excited charge carriers released from the valance band, trapping centers and pyridinic-N functional groups play more dominant roles in the thermoresistive response of the sensor than the variable-range hopping (VRH) of carriers.[26]

Figure S5. Digital image of the data logger showing no reading (OVL.D means overload) for the CNF500 TS, indicating that the electrical resistance is over 100 MΩ.

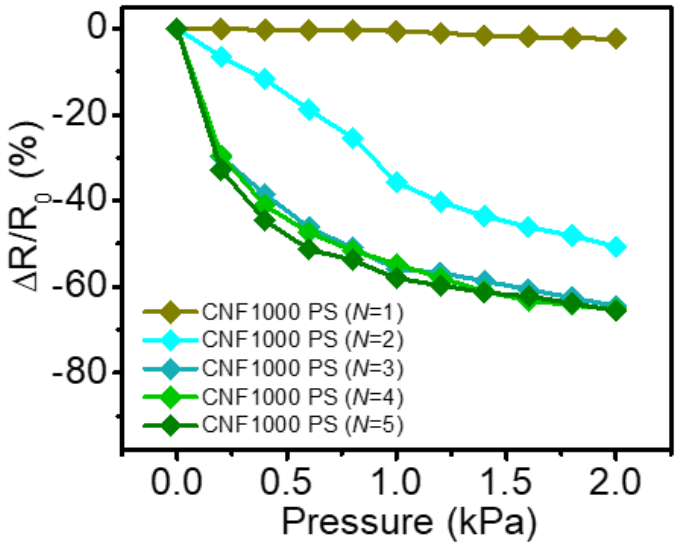

Figure S6. Pressure-dependent $\Delta R/R_0$ of the PSs made of the CNF1000 films with different number of layers (N).

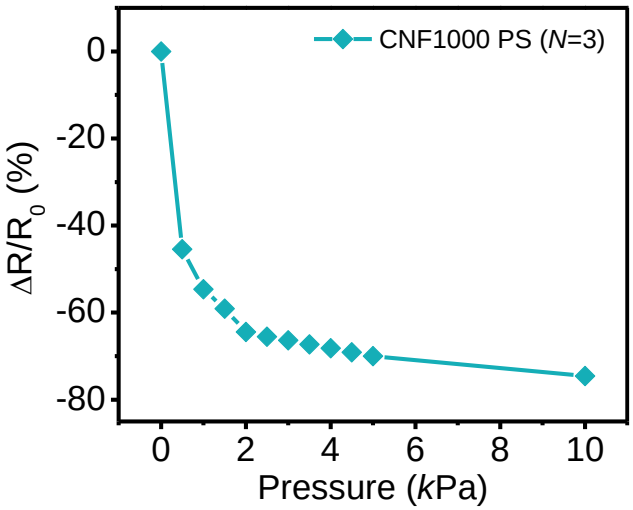

Figure S7. Pressure-dependent $\Delta R/R_0$ of the CNF1000 PS in the extended pressure range from 0 to 10 *k*Pa.

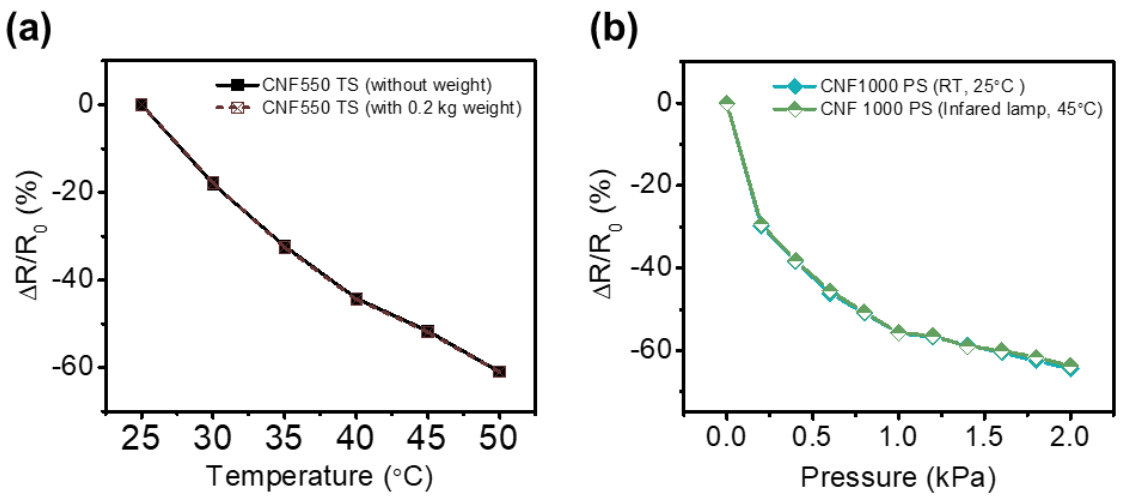

Figure S8. (a) Temperature-dependent $\Delta R/R_0$ of the CNF550 TS with and without a 0.2 kg weight on top of the sensor. (b) Pressure-dependent $\Delta R/R_0$ of the CNF1000 PS with and without infrared lamp heating.

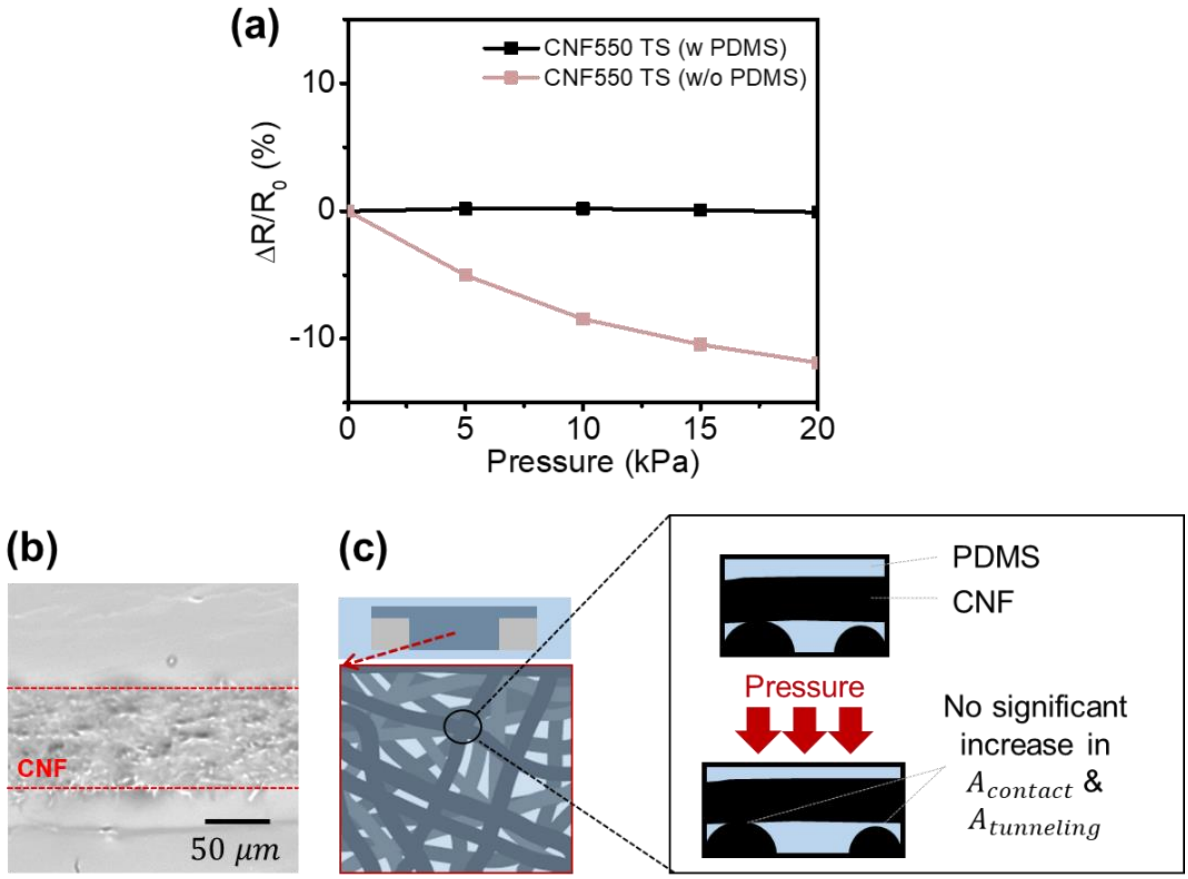

Figure S9. (a) $\Delta R/R_0$ of the CNF550 TS with and without PDMS infiltration as a function of pressure ranging 0-20 *k*Pa. (b) Cross-sectional SEM image of the CNF550 TS showing the CNF550 film encapsulated by PDMS. (c) Schematic illustration showing the pressure-insensitive mechanism of the CNF550 TS.

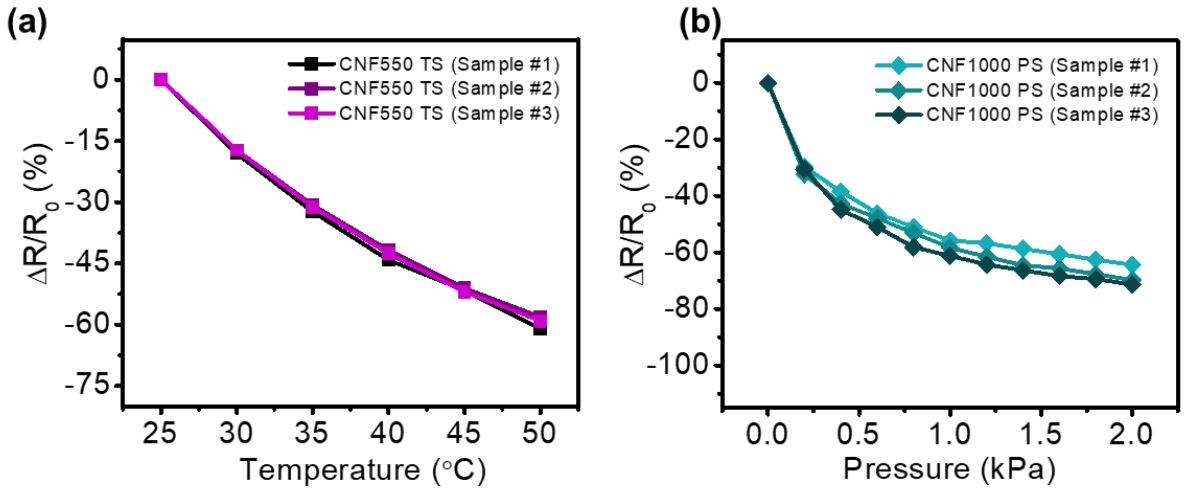

Figure S10. (a) Temperature- and (b) pressure-dependent $\Delta R/R_0$ of the multifunctional sensors made of CNF films from different electrospinning batches.

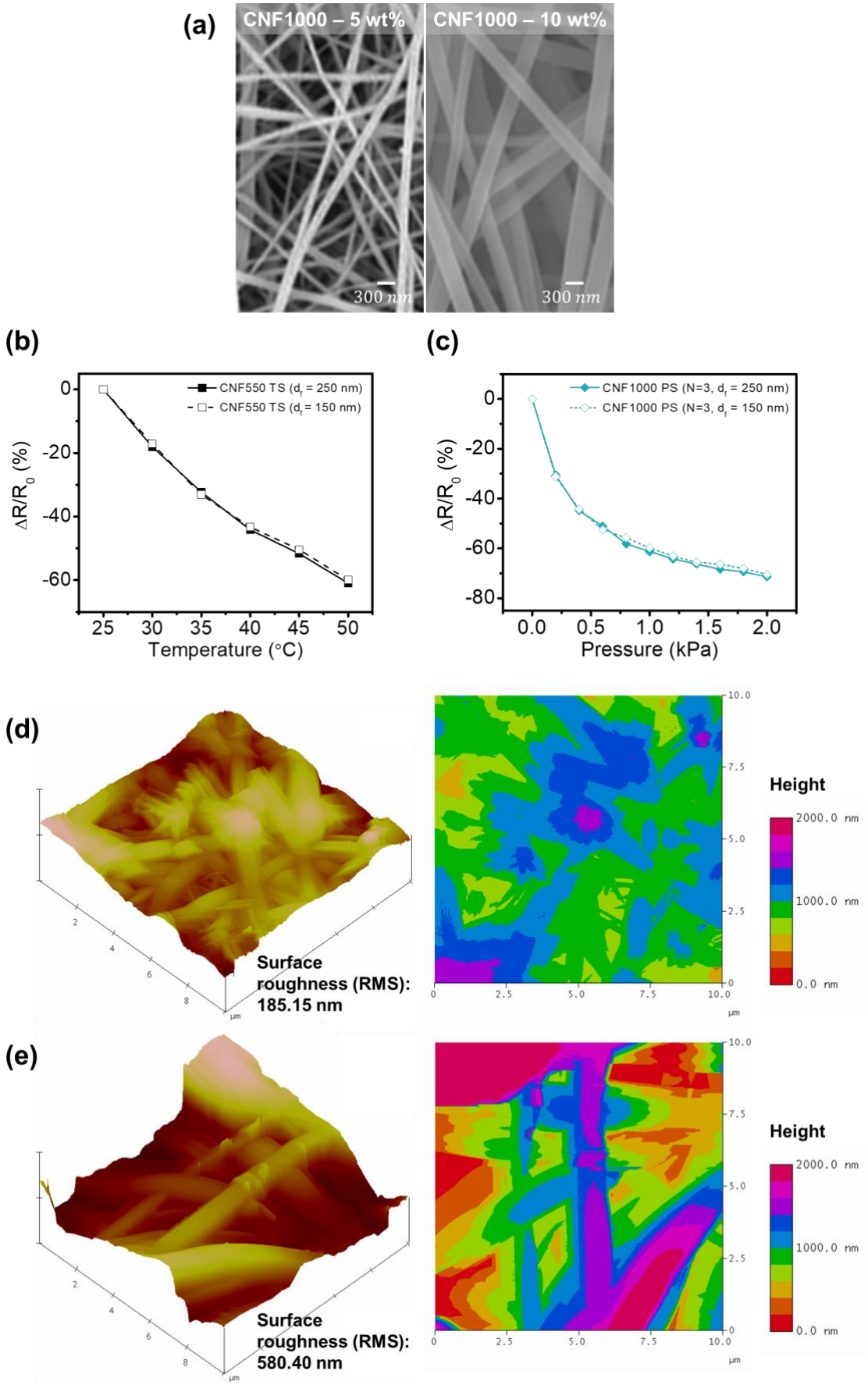

Figure S11. (a) SEM images of CNF1000 prepared from 5 and 10 wt% PAN precursor solutions, with an average fiber diameter (d_f) of 150 and 250 *nm*, respectively. (b) Temperature-dependent $\Delta R/R_0$ of the TSs made using the CNF550 films with different d_f. (c) Pressure-

dependent $\Delta R/R_0$ of the PSs made using the CNF1000 films with different d_f. Atomic force microscopy (AFM) surface profiles and height analyses of the CNFs with d_f of (d) 150 and (e) 250 *nm*.

The effect of CNF diameter on temperature and pressure sensitivities is examined. The fiber diameter is controlled by adjusting the concentration of PAN in the precursor solution, with a lower PAN concentration resulting in a smaller average fiber diameter (d_f) of the CNFs (Figure S11a). It should be noted that when the concentration of PAN is higher than 10 wt%, the electrospinning syringe needle tends to be clogged up due to the high viscosity of the precursor solution, making it impossible to spin fibers.[2] Importantly, increasing d_f has a negligible effect on improving the sensitivities of the CNF550 TS and CNF1000 PS, as shown in Figures S11b and S11c. The strong thermoresistive characteristic of the CNF550 TS sensor was mainly correlated to the atomic structures of CNFs.[26] Because the CNFs carbonized at 550 °C exhibited similar atomic structures regardless of their diameters, increasing d_f from 150 to 250 nm hardly affected the sensitivity of the CNF550 TS. Further, although the surface roughness of the CNF film can be increased with increasing d_f (Figures S11d and e), the increment is insufficient to create a noticeable change in contact area between the CNF films when a pressure is applied, thereby unable to improve the pressure sensitivity. In other words, controlling *N* is the most effective means to improve the sensitivity of the CNF1000 PS.

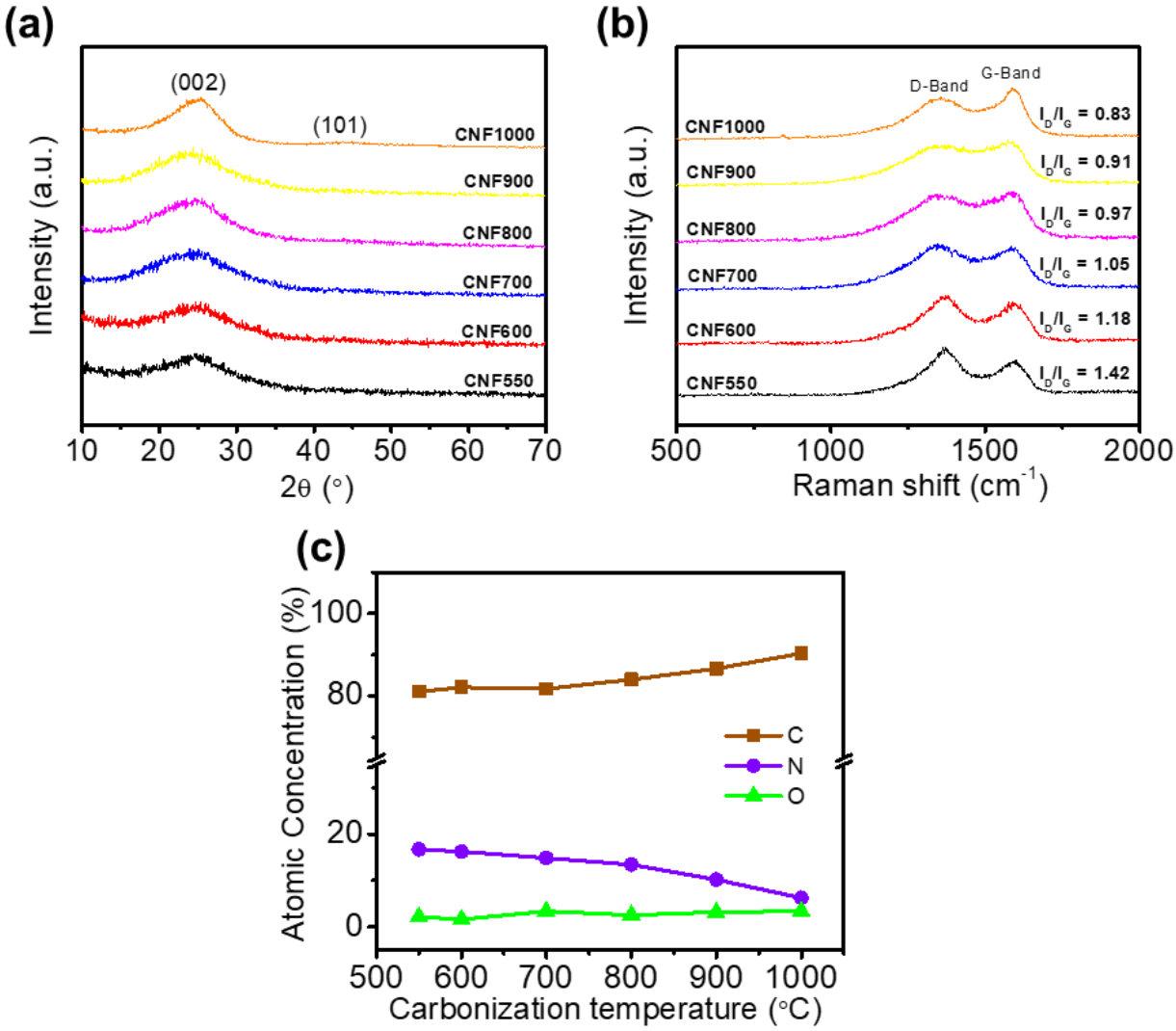

Figure S12. Structural characteristics of CNFs carbonized at different temperatures. (a) XRD patterns; (b) Raman spectra; (c) Atomic concentrations of carbon (C), nitrogen (N), and oxygen (O) in CNFs as a function of carbonization temperature.

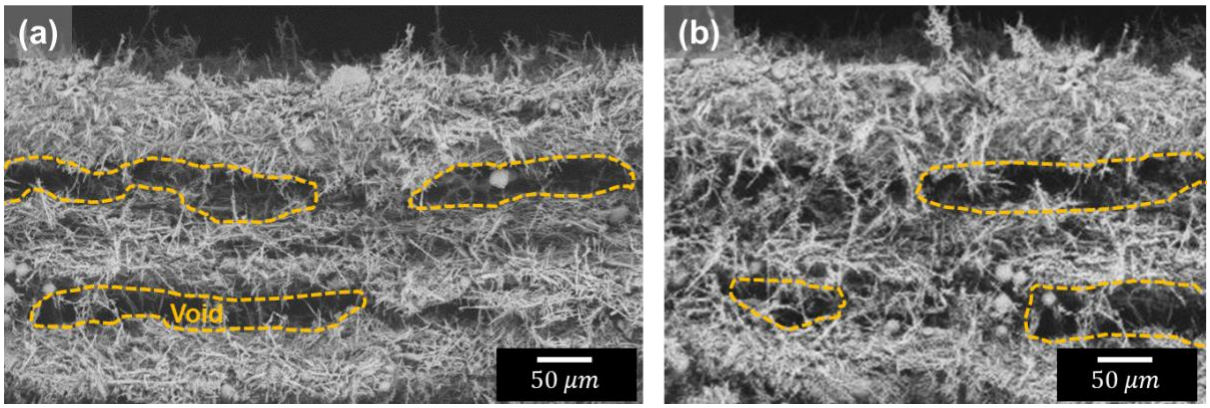

Figure S13. SEM images showing voids between the CNF films in the CNF1000 PS (a) prior to loading and (b) after 100th cyclic loading up to 10 *k*Pa.

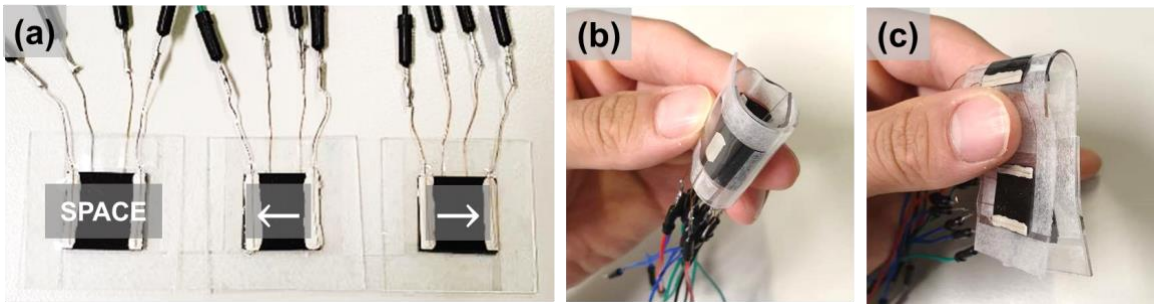

Figure S14. (a) 1 × 3 array of three CNF multifunctional sensors which work as right arrow, left arrow and space keys, respectively. Digital images showing (b) rollable and (c) flexible nature of 1 × 3 array of three CNF multifunctional sensors.

Table S1. Comparison of important features between the current CNF multifunctional sensor and other state-of-the-art multifunctional sensors with stimulus discriminability reported in the literature.

Material	Fabrication	Output signal	Methods to achieve stimulus discriminability	Readout	Temperature sensitivity	Pressure sensitivity	Ref
PEDOT:PSS/ PU composite	simple	i) voltage ii) current	thermoelectric & piezoelectric material	complex & expensive	35.5 μV °C^{-1}	28.9 *k*Pa^{-1}	[5]
rGO & pyramid shaped SWCNT-embedded PDMS	complex	i) resistance ii) capacitance	resistive temperature sensor & capacitive pressure sensor	complex & expensive	0.83 %°C^{-1}	0.7 *k*Pa^{-1}	[20]
$BaTiO_3$	simple	i) voltage	pyroelectric & piezoelectric material	complex & expensive	0.048 V °C^{-1}	0.044 V kPa^{-1}	[25]
$Bi_4Ti_3O_{12}$ & rGO	complex	i) resistance ii) voltage	thermoresistive & triboelectric material	complex & expensive	1.15 %°C^{-1}	5.07 V kPa^{-1}	[21]
CB & AgNW	complex	i) current	machine learning	complex & expensive	0.0000515 %°C^{-1}	264 kPa^{-1}	[27]
rGO/PDMS composite	simple	i) voltage ii) current	thermoelectric & piezoelectric material	complex & expensive	35.2 μV°C^{-1}	15.22 kPa^{-1}	[24]
CNT & PU	complex	i) resistance ii) capacitance	resistive temperature sensor & capacitive pressure sensor	complex & expensive	0.28 %°C^{-1}	0.753 kPa^{-1}	[29]
polyaniline composite & P(VDF-TrFE)	complex	i) voltage	thermoelectric & piezoelectric material	complex & expensive	109.4 µV °C^{-1}	0.64 V kPa^{-1}	[23]
electrospun CNF	**simple**	**i) resistance**	**thermoresistive & piezoresistive material**	**simple & low-cost**	**2.44 %°C^{-1}**	**0.96 *k*Pa^{-1}**	**This work**

CB = Carbon black
CNT = Carbon nanotube
NgNW = Silver nanowire
PDMS = Polydimethylsiloxane
PEDOT:PSS = Poly(3,4-ethylenedioxythiophene) polystyrene sulfonate
PU = Polyurethane
P(VDF-TrFE) = Poly(vinylidene fluoride-co-trifluoroethylene)
rGO = Reduced graphene oxide
SWCNT = Single-walled carbon nanotube